Supplement of Atmos. Chem. Phys., 25, 7269–7297, 2025
https://doi.org/10.5194/acp-25-7269-2025-supplement

Atmospheric Chemistry and Physics
Open Access
EGU

Supplement of

Biosphere–atmosphere related processes influence trace-gas and aerosol satellite–model biases

Emma Sands et al.

Correspondence to: Emma Sands (e.g.sands@ed.ac.uk)

BVOC emission factors

Recent work has identified that expansion of the number of plant functional types (PFTs) in the UK Earth System Model (UKESM) may have resulted in inaccurate assignment of isoprene and monoterpene emission factors (IEF and TEF, respectively) to the new PFTs (Weber et al. 2023). Table S1. illustrates the original and updated isoprene and monoterpene emission factors used in the study. In general, the new IEF and TEF values result in increased BVOC emissions from broadleaf forests and deciduous shrubs, while decreases occur elsewhere. The change is particularly substantial for C3 and C4 crop and pasture PFTs, which see a factor of 500 decrease.

Table S1. Emission factors (μgC g_{dw}^{-1} hr^{-1}) used for calculating emissions of isoprene (IEF) and (mono)terpenes (TEF) in iBVOC. The original and new EFs are marked by the subscripts 'orig' and 'new', respectively. The red font highlights EFs, which are greater than the original values, while a decrease in the EF is marked by the use of a blue font.

Plant functional type	IEF_{orig}	IEF_{new}	TEF_{orig}	TEF_{new}
Broadleaf deciduous trees	35	72.3	1.33	2.7
Broadleaf evergreen tropical trees	24	38.1	1.2	1.8
Broadleaf evergreen temperate trees	16	54.4	1.2	1.3
Needleleaf deciduous trees	8	0.01	2.40	1.8
Needleleaf evergreen trees	8	6.3	2.40	0.9
C3 grass	16	11.6	0.80	0.02
C3 crop	5	0.01	0.20	0.02
C3 pasture	5	0.01	0.20	0.02
C4 grass	24	2.20	1.70	0.02
C4 crop	5	0.01	0.20	0.02
C4 pasture	5	0.01	0.20	0.02
Shrub deciduous	10	35.2	1.25	1.3
Shrub evergreen	20	10.2	1.00	0.6

Reaction rate updates

The Arrhenius expression is used to calculate the rate coefficient for bimolecular reactions in the United Kingdom Chemistry and Aerosol (UKCA) model:

$$k = k_0 \left(\frac{T}{300}\right)^{\alpha} exp\left(\frac{-\beta}{T}\right),$$

where k_0 is the pre-exponential factor, T is the temperature, α is the exponent for the ($T/300$) temperature dependence and β represents the Arrhenius activation energy divided by the gas constant (O'Connor et al. 2014). The values of the coefficients vary depending on the reaction and are periodically updated, alongside the fractions of products produced in those reactions, to align with new published data (e.g. IUPAC Task Group on Atmospheric Chemical Kinetic Data Evaluation, http://iupac.pole-ether.fr/, last access: 25/09/2024, and Burkholder et al. (2019)).

Table S2. summarises recent updates to the coefficients used to calculate the bimolecular reaction rate coefficients. The reactions shown here are not an exhaustive list of all the updates, as other reaction types (e.g., termolecular) are also affected, but are meant to provide an overview of the changes and include key BVOC reactions. The impacts of these updates are studied in *Exp_RR*.

Table S2. Updates to values used to calculate the rate coefficient for bimolecular reactions in the Strat-Trop scheme.

Reaction	k0		alpha		beta		other comments	Diff at given T	
	old	new	old	new	old	new		276 K	283 K
C5H8+O3->HO2+OH	3.33E-15	3.30E-15	0	0	1995	2000		97%	97%
C5H8+O3->MACR+HCHO+MACRO2+MeCO3	3.33E-15	3.30E-15	0	0	1995	2000		97%	97%
C5H8+O3->MeOO+HCOOH+CO+H2O2	3.33E-15	3.30E-15	0	0	1995	2000		97%	97%
C5H8+OH->ISO2	2.70E-11	3.00E-11	0	0	-390	-390		111%	111%
C5H8+NO3->ISON	3.15E-12	2.95E-12	0	0	450	450		94%	94%
C10H16+O3->sec_org	1.01E-15	8.22E-16	0	0	732	640		114%	113%
C10H16+OH->sec_org	1.20E-11	1.34E-11	0	0	-444	-410		99%	99%
C10H16+NO3->sec_org	1.19E-12	1.20E-12	0	0	-925	-490		21%	22%
BrO+BrO-> Br+Br+O2	2.40E-12	1.50E-12	0	0	-40	-230		124%	122%
CFCl3+O(1D)-> Cl+Cl+ClO	2.30E-10	2.07E-10	0	0	0	0		90%	90%
CF2Cl2+O(1D)-> Cl+ClO	1.40E-10	1.20E-10	0	0	0	-25		94%	94%
Cl+CH4->HCl+MeOO	6.60E-12	7.10E-12	0	0	1240	1270		96%	97%
Cl+H2->HCl+H	3.90E-11	3.05E-11	0	0	2310	2270		90%	90%
Cl+HO2->ClO+OH	4.10E-11	3.60E-11	0	0	450	375		115%	114%
ClO+MeOO->Cl+HCHO+HO2	3.30E-12	1.80E-12	0	0	115	600		9%	10%
ClO+NO3->Cl+O2+NO2	4.60E-13	4.70E-13	0	0	0	0		102%	102%
EtOO+NO->MeCHO+HO2+NO2	2.55E-12	2.60E-12	0	0	-380	-365		97%	97%
H+NO2->OH+NO	4.00E-10	1.35E-10	0	0	340	0		116%	112%
HO2+EtCO3->O2+EtCO3H	4.40E-13	1.76E-13	0	0	-980	-1040		50%	49%
HO2+EtCO3->O3+EtCO2H	7.80E-14	6.45E-14	0	0	-980	-1040		103%	102%

HO2+MeCO3->MeCO2H+O3	7.80E-14	2.25E-13	0	0	-980	-730	117%	119%
HO2+MeCO3->MeCO3H	2.13E-13	6.40E-13	0	0	-980	-730	121%	124%
HO2+MeCO3->OH+MeOO	2.29E-13	8.65E-13	0	0	-980	-730	153%	156%
HO2+MeCOCH2OO->MeCOCH2OOH	9.00E-12	8.60E-13	0	0	0	-700	121%	113%
HO2+NO->OH+NO2	3.30E-12	3.44E-12	0	0	-270	-260	101%	101%
HO2+O3->OH+O2	2.03E-16	1.00E-14	4.57	0	-693	490	99%	98%
MeBr+Cl->Br+HCl	1.40E-11	1.46E-11	0	0	1030	1040	101%	101%
Mebr+OH->Br+H2O	2.35E-12	1.42E-12	0	0	1300	1150	104%	103%
MeCO3+NO->MeOO+CO2+NO2	7.50E-12	8.10E-12	0	0	-290	-270	100%	101%
MeCOCH2OO +NO->MeCO3+HCHO+NO2	2.70E-12	2.90E-12	0	0	-360	-300	86%	87%
MeOO+MeOO->HO2+HO2+HCHO+HCHO	1.03E-13	1.03E-13	0	0	-365	-390	109%	109%
MeOO+MeOO->MeOH+HCHO	1.03E-13	1.03E-13	0	0	-365	-390	109%	109%
MeOO+NO->HO2+HCHO+NO2	2.30E-12	2.80E-12	0	0	-360	-300	98%	98%
MeOO+NO->MeONO2	2.30E-15	8.97E-15	0	0	-360	-360	390%	390%
N+O2->NO+O(3P)	1.50E-11	3.30E-12	0	0	3600	3150	112%	108%
NO+ISO2->ISON	1.12E-13	9.68E-13	0	0	-360	0	235%	242%
NO+ISO2->NO2+MACR+HCHO+HO2	2.43E-12	7.83E-12	0	0	-360	0	87%	90%
NO+MACRO2->MGLY+HCHO+HO2	1.27E-12	1.35E-12	0	0	-360	-360	106%	106%
NO+MACRO2->NO2+MeCO3+HACET	1.27E-12	1.25E-12	0	0	-360	-360	98%	98%
NO+NO3->NO2+NO2	1.50E-11	1.70E-11	0	0	-170	-125	96%	97%
NO2+NO3->NO+NO2+O2	4.50E-14	4.35E-14	0	0	1260	1340	72%	73%
no3+hcho->hono2+ho2+co	2.00E-12	5.80E-16	0	0	2440	0	200%	161%
NO3+MGLY->MeCO3+CO+HONO2	3.36E-12	5.00E-16	0	0	1860	0	13%	11%
O(1D)+CH4->HCHO+H2	9.00E-12	8.75E-12	0	0	0	0	97%	97%
O(1D)+CH4->HCHO+HO2+HO2	3.45E-11	3.50E-11	0	0	0	0	101%	101%
O(1D)+HBr->OH+Br	1.20E-10	9.00E-11	0	0	0	0	75%	75%
O(1D)+HCl->H+ClO	3.60E-11	3.30E-11	0	0	0	0	92%	92%
O(1D)+HCl->O(3P)+HCl	1.35E-11	1.80E-11	0	0	0	0	133%	133%
O(1D)+HCl->OH+Cl	1.01E-10	9.90E-11	0	0	0	0	98%	98%
O(1D)+N2O->N2+O2	4.60E-11	4.64E-11	0	0	-20	-20	101%	101%
O(1D)+N2O->NO+NO	7.30E-11	7.26E-11	0	0	-20	-20	99%	99%
O(3P)+HO2->OH+O2	2.70E-11	3.00E-11	0	0	-224	-200	102%	102%
O(3P)+NO2->NO+O2	5.10E-12	5.30E-12	0	0	-210	-200	100%	100%
O(3P)+NO3->O2+NO2	1.70E-11	1.30E-11	0	0	0	0	76%	76%
O3+MACR->MGLY+HCOOH+HO2+CO	2.13E-16	1.23E-15	0	0	1520	2100	71%	74%

O3+MACR->OH+MeCO3	2.13E-16	1.68E-16	0	0	1520	2100		10%	10%
OH+C3H8->H2O+EtOO	6.90E-12	7.66E-12	0	0	1000	1020		103%	103%
OH+C3H8->i-PrOO+H2O	7.60E-12	6.76E-12	0	0	585	630		76%	76%
OH+C3H8->n-PrOO+H2O	7.60E-12	2.43E-12	0	0	585	630		27%	27%
OH+CO->H+CO2	1.44E-13	1.85E-13	0	0	0	65		102%	102%
OH+H2->H2O+HO2	2.80E-12	2.80E-12	0	0	1800	1800	products changed to H2O+H	100%	100%
OH+HACET->MGLY+HO2	1.60E-12	2.00E-12	0	0	-305	-320		132%	132%
OH+HCHO->H2O+HO2+CO	5.40E-12	5.50E-12	0	0	-135	-125		98%	98%
OH+HCOOH->HO2	4.50E-13	4.00E-13	0	0	0	0	products changed to CO2+H2O+H	89%	89%
OH+HO2NO2->H2O+NO2+O2	3.20E-13	4.50E-13	0	0	-690	-610		105%	106%
OH+HONO->H2O+NO2	2.50E-12	3.00E-12	0	0	-260	-250		116%	116%
OH+HONO2->H2O+NO3	2.40E-14	3.70E-14	0	0	-460	-240		69%	71%
OH+MeCHO->H2O+MeCO3	4.70E-12	4.63E-12	0	0	-345	-350		100%	100%
OH+MeCO2H->MeOO	8.00E-13	3.15E-14	0	0	0	-920		110%	102%
OH+MeOH->HO2+HCHO	2.85E-12	2.90E-12	0	0	345	345		102%	102%
OH+MeONO2->HCHO+NO2+H2O	4.00E-13	8.00E-13	0	0	845	1000		114%	116%
OH+MeOOH->H2O+HCHO+OH	2.12E-12	1.10E-12	0	0	-190	-200		54%	54%
OH+MeOOH->H2O+MeOO	1.89E-12	2.70E-12	0	0	-190	-200		148%	148%
OH+NO3->HO2+NO2	2.20E-11	2.00E-11	0	0	0	0		91%	91%
OH+OH->H2O+O(3P)	6.31E-14	1.80E-12	2.6	0	-945	0		115%	118%
i-PrOO+NO3->Me2CO+HO2+NO2	2.70E-12	2.20E-12	0	0	-360	0		22%	23%
n-PrOO+NO3->EtCHO+HO2+NO2	2.70E-12	2.30E-12	0	0	-360	0		23%	24%
CS2+O(3P)->COS+SO2+CO	3.20E-11	3.30E-11	0	0	650	650	products updated to CO+SO2+SO2	103%	103%
CS2+OH->COS+SO2	1.25E-16	2.00E-15	0	0	-4550	0		0%	0%
DMS+OH->SO2	1.20E-11	1.20E-11	0	0	260	280		93%	93%
DMS+NO3->SO2	1.90E-13	1.90E-13	0	0	-500	-530		111%	111%
DMSO+OH->SO2+MSA	5.80E-11	6.10E-12	0	0	0	-800		191%	178%
H2S+O(3P)->OH+SO2	9.20E-12	9.20E-12	0	0	1800	1800	products updated to OH+SO2+OH+O(3P)	100%	100%
H2S+OH->SO2+H2o	9.20E-12	9.20E-12	0	0	75	-100		189%	186%
COS+OH->CO2+SO2	1.10E-13	7.20E-14	0	0	1200	1070		105%	104%
ISO2+RO2->MACR+HCHO+HO2	1.67E-12	1.26E-12	0	0	0	0		75%	75%
MACRO2+RO2->HACET+MGLY+HCHO+CO	8.37E-13	2.10E-13	0	0	0	0		25%	25%
MACRO2+RO2->HO2	8.37E-13	2.10E-13	0	0	0	0		25%	25%

Isoprene vertical distribution in the model for comparison against CrIS retrieval

Satellite retrievals of atmospheric trace gases are not uniformally sensitive across different layers of the atmosphere. Figure S1 shows the average vertical distribution of isoprene volume mixing ratios in the troposphere in South America, which highlights how most of the trace gas simulated by the model is found in the lower troposphere (>800 hPa). The averaging kernel for an example satellite retrieval of isoprene from within the same region shows that the retrievals are sensitive to the lower troposphere, particularly at around 900hPa (Fu et al., 2019). Therefore, despite the lack of detailed information on the vertical sensitivity of the observational data used in the study, we suggest using the satellite isoprene dataset is appropriate for identifying total column model biases.

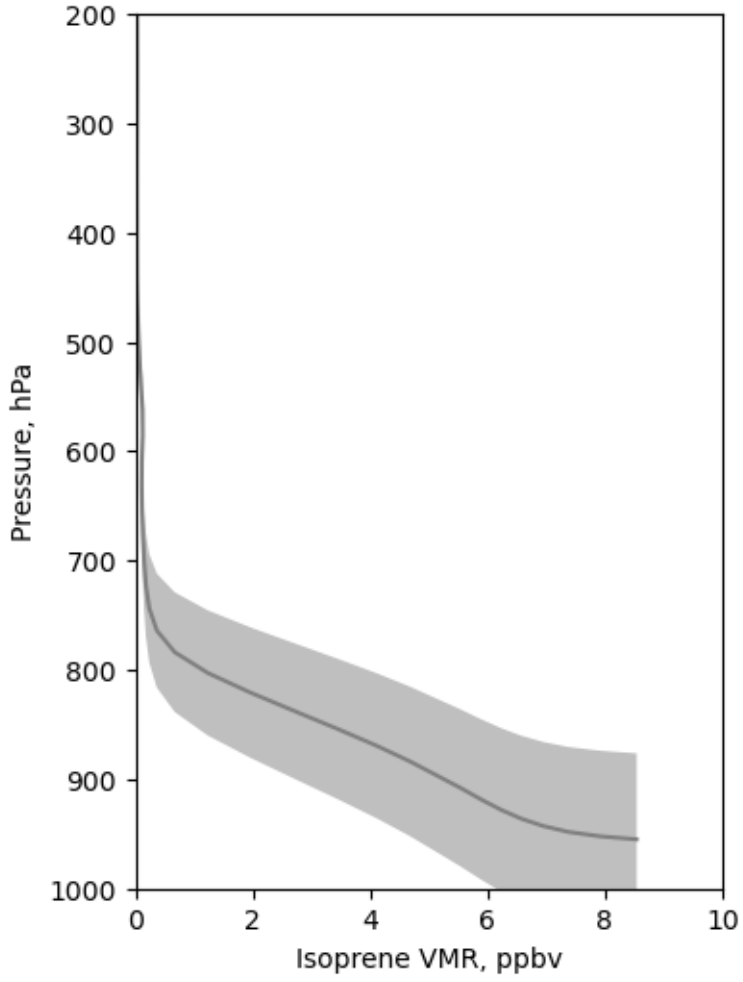

Figure S1. Mean vertical distribution of isoprene (VMR) in South America (0 to 15 degrees S, 60 to 80 degrees W) in September 2014. Cf isoprene retrieval and averaging kernels in Fu et al. (2019), Figure 4.

Impacts of using different time profiles for model data analysis for satellite-model comparison

Isoprene emissions and the concentrations of oxidants in the atmosphere are known to have daily cycles. Consequently, isoprene total column values at a given location will fluctuate daily, with implications for comparing model output to satellite observations. Figure S2 illustrates the difference between mean total column isoprene values calculated for February to December 2012 using two sets of model outputs. The first set is based on data that has been output every 6 hours and subsequently filtered to use those outputs closest in time to the satellite overpass on a given day at a given location before the monthly mean value is calculated. A second simulation output daily data within one hour of the satellite overpass time of 13:30 LT. For this purpose, 12 longitudinal domains were created, which enabled the output of data at 13:30 LT in the middle and at the edges of the domain. Linear interpolation was used to obtain values for approximately 13:30 LT for the cells in between. These data form the basis of the second set of monthly mean data.

A comparison of model outputs for December, March, June and September (Fig. S2 d-g) shows the areas primarily affected by the choice of time profile remain relatively consistent throughout the year. In the north and northwest of South America the values are greater by >1.2 × 10^{16} molec. cm^{-2} when the 13:30 LT outputs are used. In the tropical and southern hemisphere Africa differences are most widespread in December and March. The annual mean difference remains <1 × 10^{16} molec. cm^{-2}. In northern Australia, parts of tropical east Asia and along the Andes, the isoprene columns are greater when the 6 hourly method is used, but only for part of the year.

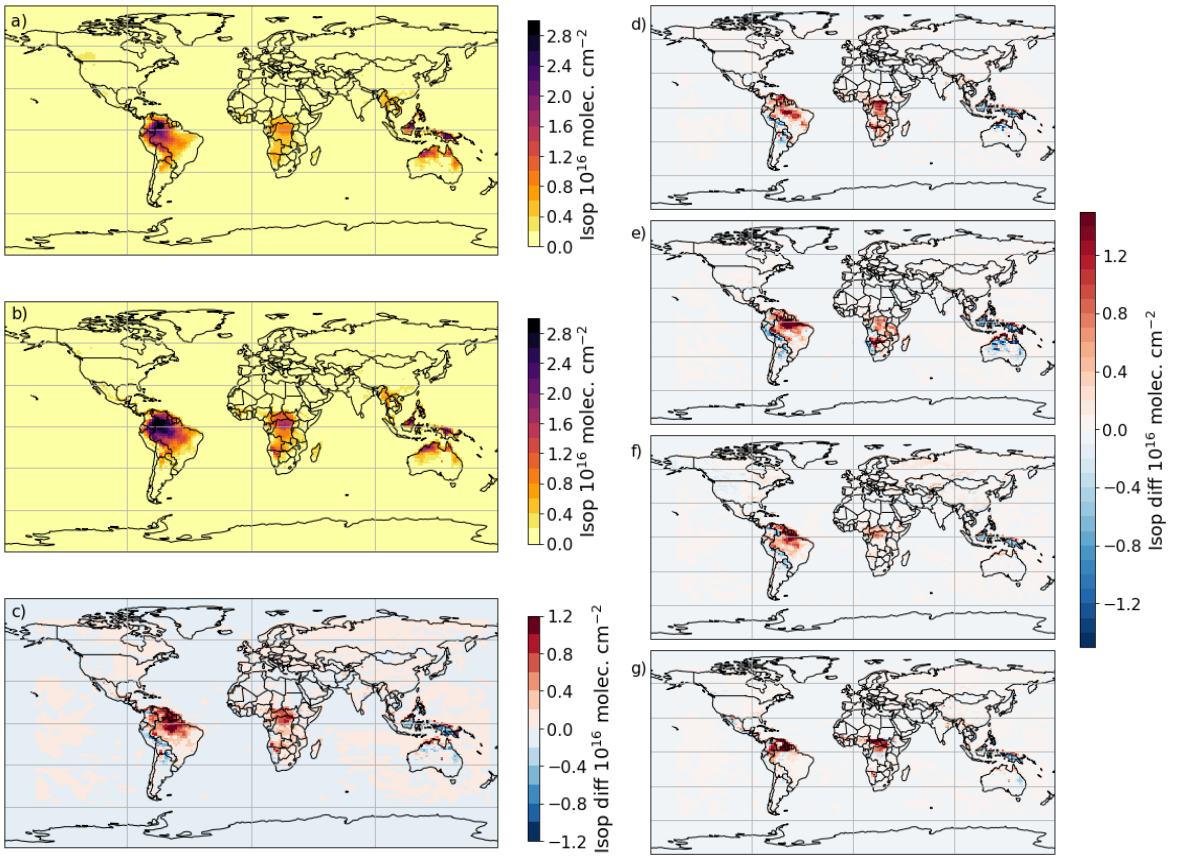

Figure S2. Comparison of the temporal means (February - December 2012) of the model output: data closest to satellite overpass time selected from 6 hourly model output (a) and model output for 13:30 LT (b). The difference (13:30 LT data – 6 hourly data) of the temporal means is presented in panel (c). Differences for December, March, June and September 2012 are presented in panels d, e, f and g, respectively.

Impact of dimethyl sulphide chemistry in CS2 on AOD

The comparison of seasonal AOD average values between the model experiment using the more complex CS2 mechanism and the baseline shows a widespread decrease in AOD values over the Southern Ocean in SON and DJF. We run an additional 2-year experiment, which isolates the impact of the dimethyl sulphide (DMS) chemistry representation on AOD values. This experiment uses the CS2 mechanism, except for the DMS reactions, which match those used in ST. Figure S3 shows the impacts on annual average AOD for 2006. When compared to the baseline, the substantial increase over China (> +0.045), alongside smaller magnitude increases above other regions of anthropogenic emissions, is highlighted. However, the Southern Ocean decrease does not occur. On the other hand, comparing the CS2 with ST DMS results to the original CS2 AOD shows an increase in Southern Ocean AOD by 0.005 to 0.015. Consequently, we attribute the difference in Southern Ocean AOD between the CS2 and ST mechanism to their representations of DMS chemistry.

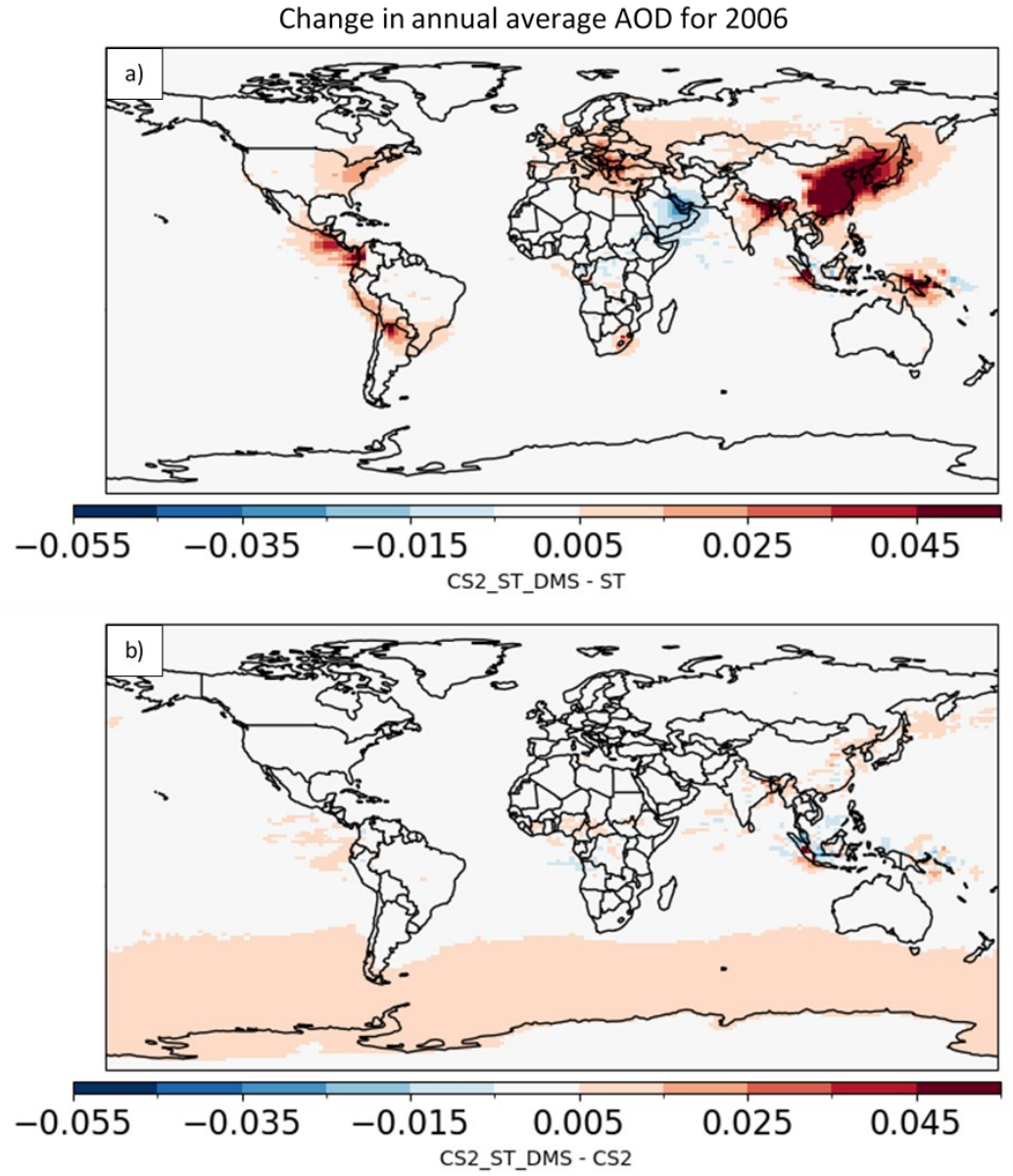

Figure S3. Difference in average AOD values for 2006 when the CS2 mechanism is used with the ST DMS scheme compared to the baseline (CS2_ST_DMS – ST, panel a) and the standard CS2 set up (CS2_ST_DMS – CS2, panel b).

Binary homogenous nucleation rate in the baseline and percentage change in Exp_CS2

Binary homogenous nucleation preferentially occurs in UKESM in the upper troposphere (Fig. S4). Changes to the concentrations of various oxidants and other chemical species driven by the more complex chemistry of the CRI-Strat 2 (CS2) mechanism can influence the rate of nucleation. We find that the nucleation rates in the upper troposphere, where most of the nucleation takes place, decrease by up to 40% compared to the Strat-Trop mechanism. Despite increases elsewhere, the lower rates in the key upper tropospheric regions result in global decrease in binary homogenous nucleation when the CS2 mechanism is used.

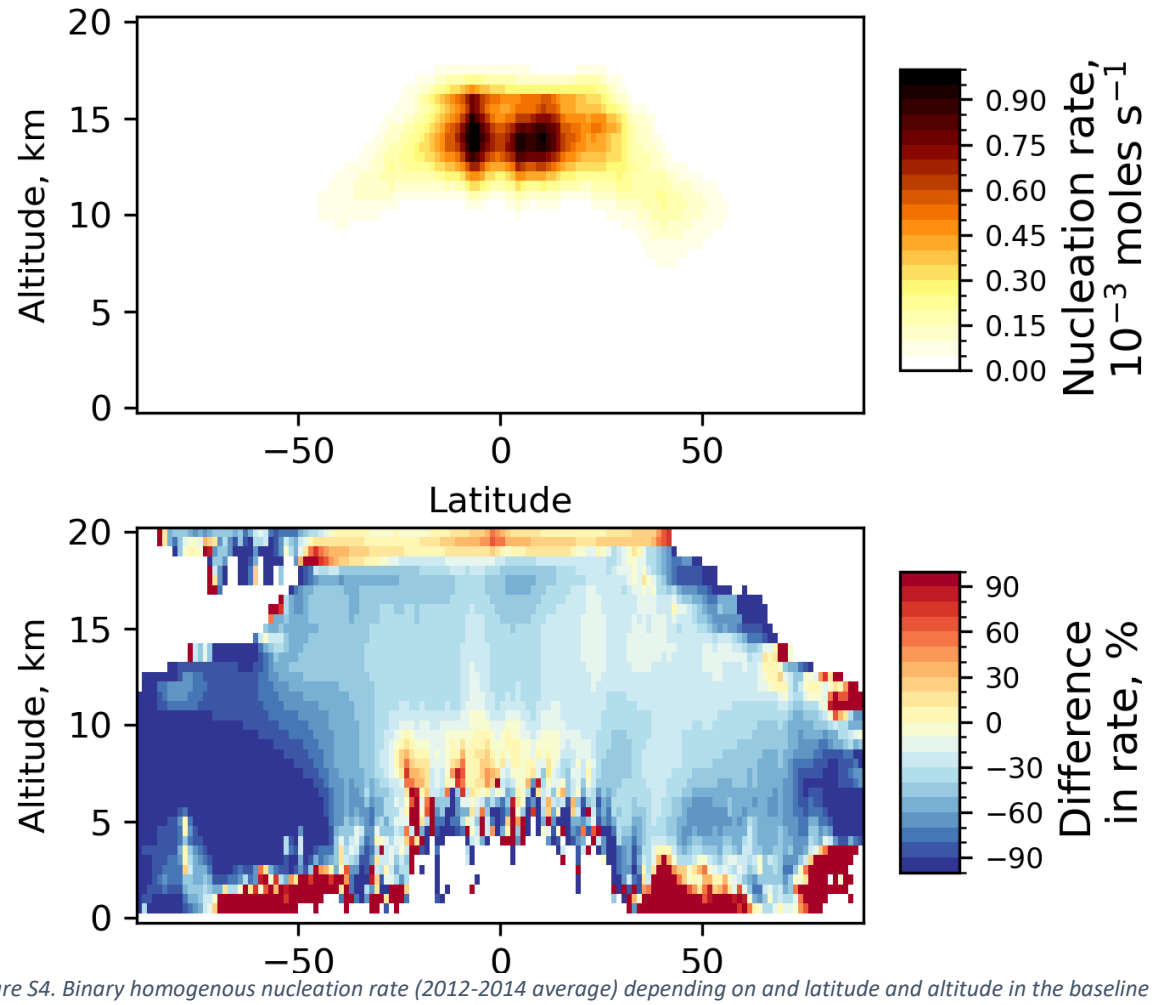

Figure S4. Binary homogenous nucleation rate (2012-2014 average) depending on and latitude and altitude in the baseline model (top). Difference in the binary homogenous nucleation as a percentage of the baseline rate, when the CS2 mechanism is used (bottom).

Aerosol size distribution in CS2

Figure S5a shows how the global aerosol size distribution (inclusive of all types of aerosols and the whole atmosphere) responds to the processes described above. Globally, the decrease is most pronounced (<-30%) for small particle sizes (Fig. S5b). The decrease in the accumulation mode, which is greater than 20% for some aerosol radii, is substantial enough to influence the accumulation-mode-sensitive AOD values. The aerosol numbers in the coarse mode are not substantially affected. The AOD response in East Asia is unusual, as values tend to increase compared to the baseline when the CS2 mechanism is used (Fig 6i). Isolating the changes in aerosol over the East Asia region, as defined by the Task Force on Hemispheric Transport of Air Pollution (TF HTAP), shows there are some positive changes for large particle numbers (Fig. S5c,d). The positive AOD change affects only part of the East Asia HTAP region, therefore a clearer signal may be found, if the data were further subset.

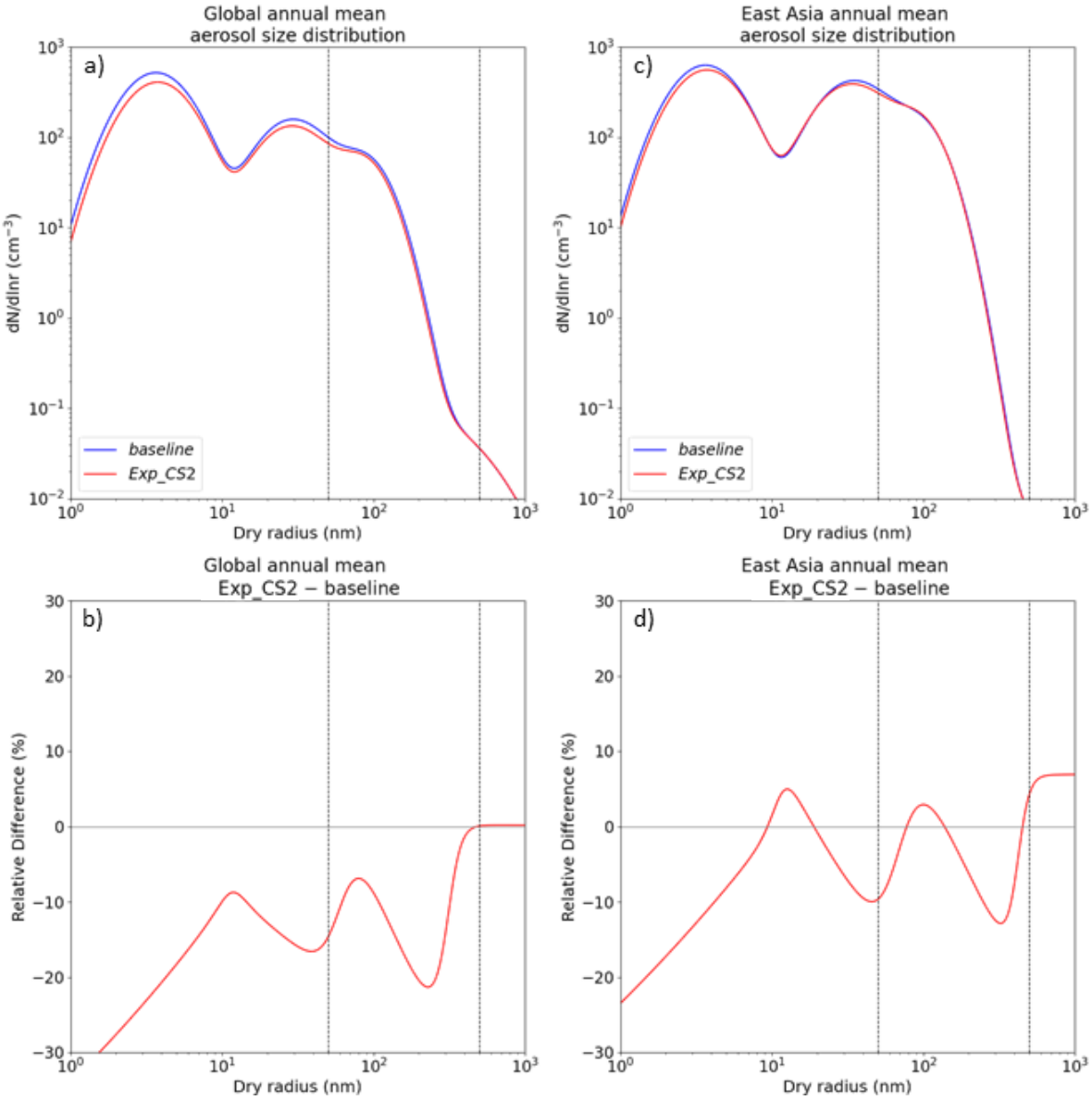

Figure S5. The 2006-2014 aerosol size distribution (blue line) in the baseline and when the more complex CS2 mechanism is used (red line) globally (a) and the difference between them (CS2-baseline) (b), as well as the same information for east Asia (c,d, using the Task Force on Hemispheric Transport of Air Pollution (TF HTAP) region definition). The vertical dashed lines indicate the typical range of aerosol radii within the accumulation mode.

Changes in grassland plant function type categories in observation-based data

Figure S6 shows the differences in the fraction of grasses, as well as crops and pastures, between the ESA CCI land cover data and the model-derived plant functional type (PFT) distribution. The original land cover types in the observational dataset are not identical to the model PFTs, resulting in some simplifications to enable the data to be used as model input.

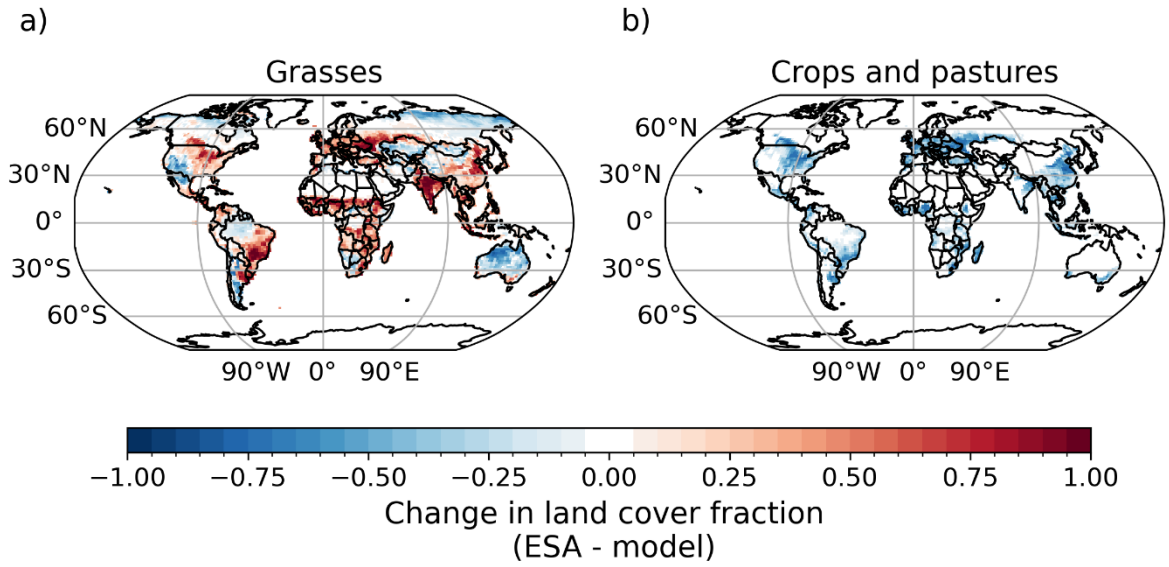

Figure S6. Change in PFT fractions between land cover derived from a free running simulation and the ESA CCI land cover ancillary. Grasses (a) includes just the C3 and C4 grass PFTs, while C3 and C4 crop and pasture PFTs are shown on subplot b.

Changes in aerosol mass and number depending on mode

Figure S7 shows the changes in aerosol mass and number separated by aerosol mode and the studied process(es). We find that as the total aerosol number increases, the total aerosol mass also tends to rise (Fig. S7 left). One exception is the accumulation mode, where aerosol mass decreases for all processes compared to the baseline, but the aerosol number increases when either of BLN or Sec_Org$_I$ formation are included. In most cases, the total aerosol mass and number increase for the Aitken insoluble mode compared to the baseline (by <30%), while the total aerosol mass decreases for the accumulation mode (by <20%). This suggests that the decrease in AOD values when BLN and Sec_Org$_I$ formation are included is driven by a shift in the aerosol size distribution, with less mass in the accumulation mode in favour of some of the smaller modes as noted in section 3.3. The more complex chemistry scheme in isolation produces a different effect as it results in lower aerosol mass and number for all aerosol modes except for the coarse mode. We note that significant changes in the organic matter aerosols do not always translate to substantial differences in total aerosol mass. This is particularly visible for the coarse mode mass, which decreases by at least 10% for organic matter, but is unchanged for total aerosol (Fig. S7 right).

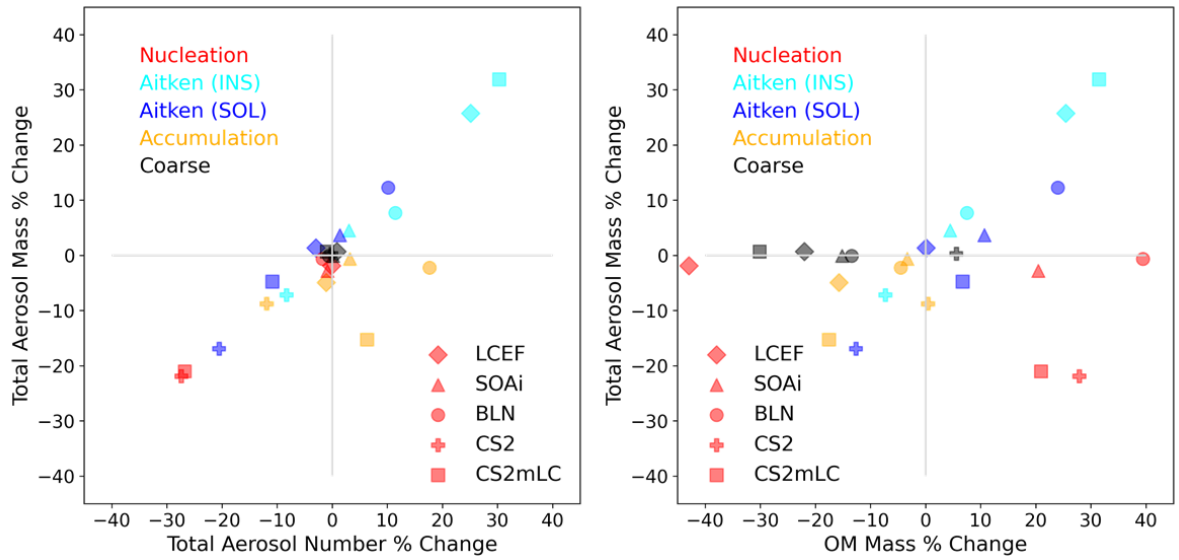

Figure S7. Percentage change from the baseline in total aerosol mass and number (left) and total aerosol mass and OM aerosol mass (right) in different aerosol size modes for four experiments.

Relative bias difference and the impact of applying averaging kernels onto model HCHO

Figure S8 shows the new model bias as a percentage of the bias calculated for the baseline model version. The data used to calculate the relative change is the same as that displayed in Fig. 14-16 in the main paper.

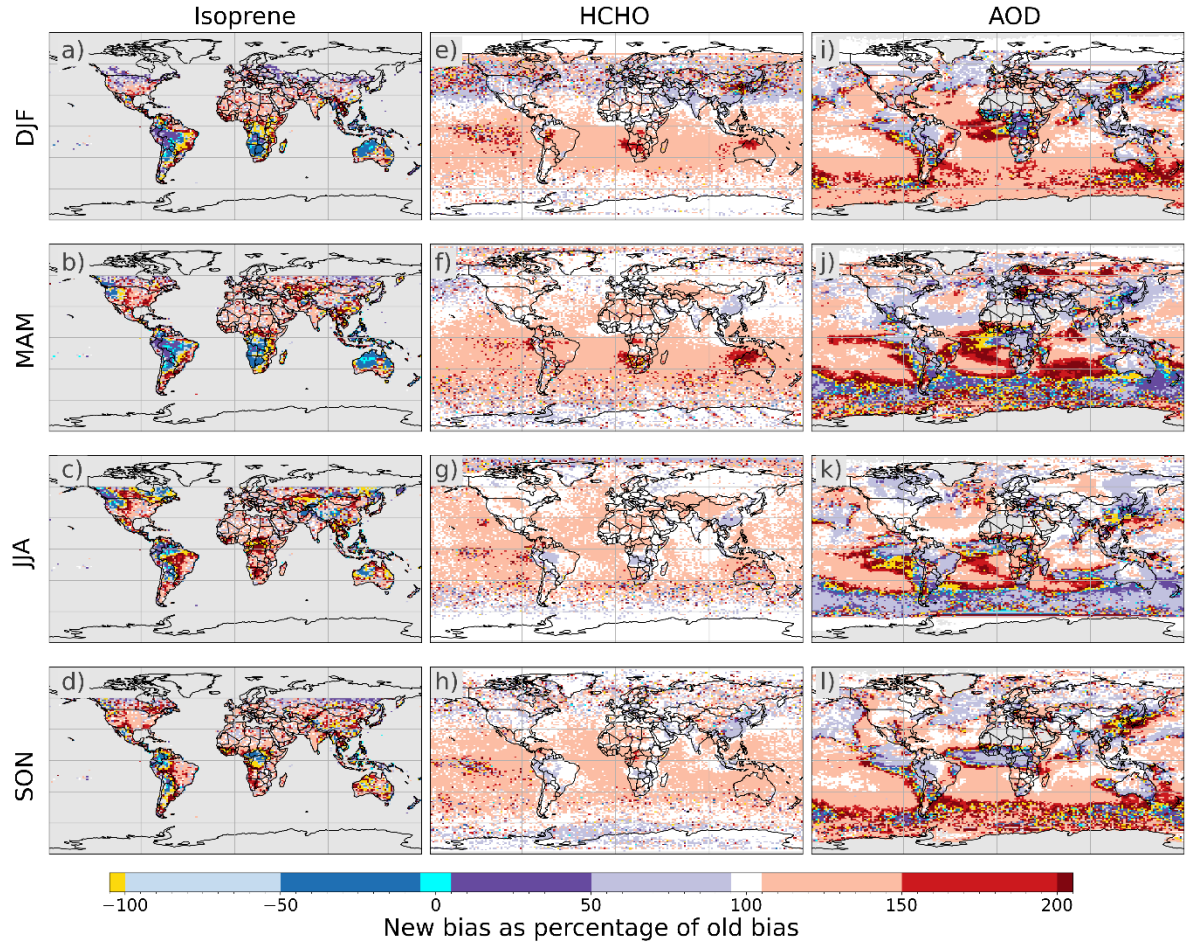

Figure S8. Satellite-model bias for Exp_CS2mLC as a percentage of the baseline model bias. 0 indicates complete 'mitigation' of the bias. Negative values indicate a change in the sign of the bias. Values over 100 (or less than -100) show the bias has increased in magnitude. The grey colour indicates no satellite data was available for a given location. Left column – isoprene, middle – HCHO, right – AOD.

Figure S9 shows the impact of applying the averaging kernels, required for accurate model-satellite comparisons, to the simulated HCHO in the baseline and when the processes are combined (Exp_CS2mLC). When the model data is interpolated onto satellite pressure levels (int, blue lines on Fig. S9), the greatest impact of the new and updated processes is found at around 800 to 900 hPa. However, once the data is multiplied by the averaging kernels (ak, red lines on Fig. S9), these differences decrease due to the low sensitivity of the satellite retrieval to the lower troposphere. Over BVOC source regions, such as the Amazon (Fig. S9b), this effect may be further exacerbated, as the upper-tropospheric decrease in HCHO is amplified. This enhancement of the high-altitude decrease combined with the low sensitivity to the low-altitude HCHO may contribute to the increase in South American bias magnitudes in DJF and MAM.

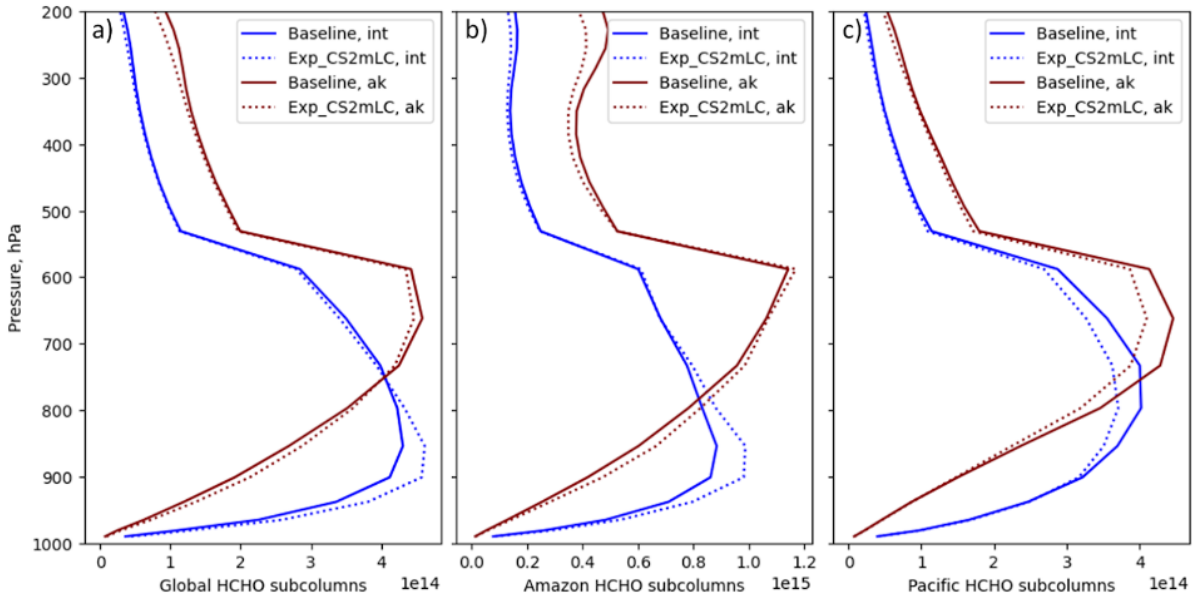

Figure S9. Impact of applying averaging kernels (ak) onto model HCHO interpolated onto satellite pressure levels (int) for the baseline (solid line) and Exp_CS2mLC (dashed line) on the global average (a), over the Amazon (a BVOC emission region: 0 to 30°S, 60 to 90°W, b) and over the Pacific Ocean (background region: 0 to 30°S, 120 to 150°W, c).

Aerosol-cloud interactions

Figure S10 shows the cloud radiative effect (CRE) in the baseline simulation (Fig. S10 a,b) and the difference in CRE when the biosphere-atmosphere processes studied in this research are included. Fig. S10 c,d does not include the impact of ESA CCI land cover due to the land cover change resulting in differences in the surface albedo. Note that areas of statistically significant differences are marked by stippling, so the inclusion of additional processes did not have a statistically significant impact over most of the globe in the nudged present-day scenario studied. Despite this there is a significant difference in the global average CRE based on the standard errors of the global mean values. The results suggest the biosphere-atmosphere processes can impact the properties of high-latitude clouds (Fig. S10 c). These effects will be studied in more detail in future work.

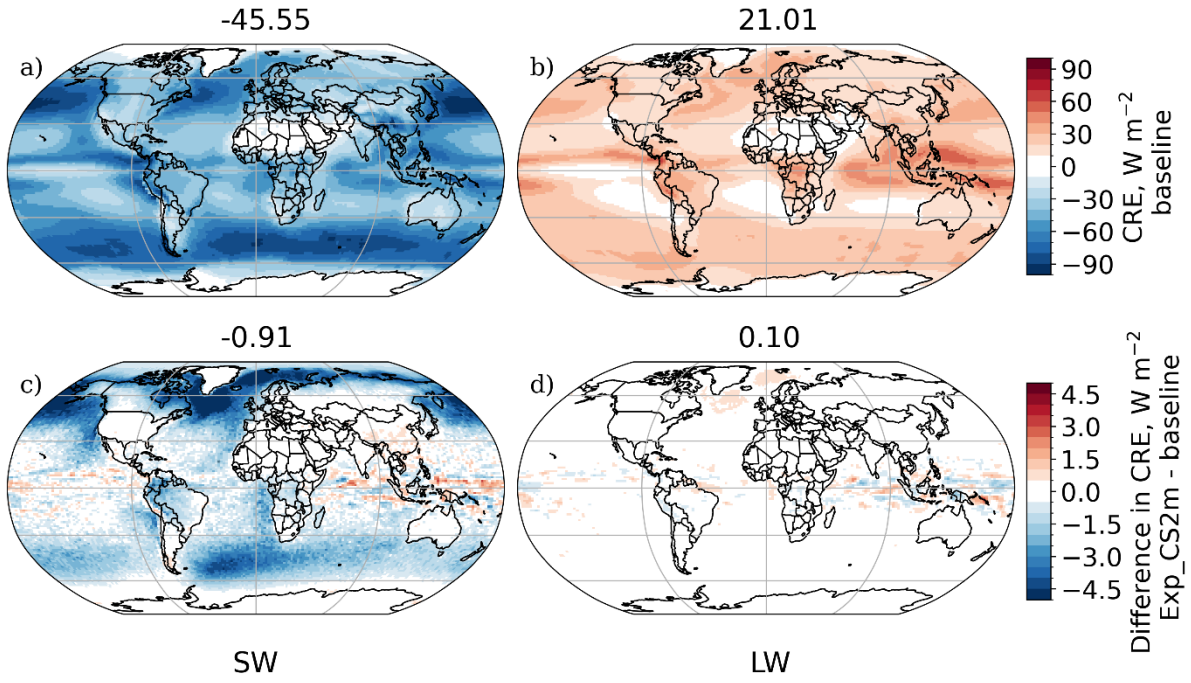

Figure S10. The cloud radiative effect in the baseline simulation for shortwave (SW, a) and longwave (LW, b) fluxes, as well as the impact of including the biosphere-atmosphere process without observation-based land cover (c,d). Stippling marks areas of statistically significant differences. The values show the global average for the given subplot.